analytical chemistry

pubs.acs.org/ac

Article

Polyhedral Particles with Controlled Concavity by Indentation Templating

Daniel W. Weisgerber, Makiko Hatori, Xiangpeng Li, and Adam R. Abate*

Cite This: *Anal. Chem.* 2022, 94, 7475−7482

Read Online

ACCESS | Metrics & More | Article Recommendations

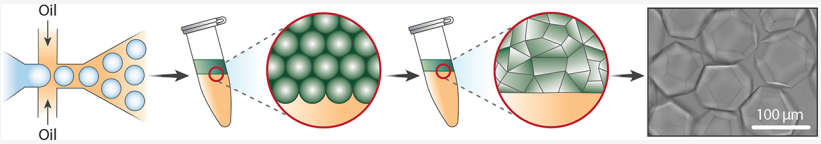

ABSTRACT: Current methods for fabricating microparticles offer limited control over size and shape. Here, we demonstrate a droplet microfluidic method to form polyhedral microparticles with controlled concavity. By manipulating Laplace pressure, buoyancy, and particle rheology, we generate microparticles with diverse shapes and curvatures. Additionally, we demonstrate the particles provide increased capture efficiency when used for particle-templated emulsification. Our approach enables microparticles with enhanced chemical and biological functionality.

INTRODUCTION

Microparticles are important for applications ranging from encapsulation and delivery of therapeutics to acting as abrasive agents in cosmetics.[1,2] They can be made from a variety of materials including proteins, polymers, ceramics, and metals with sizes ranging from 1 to 1000 μm.[1,3,4] Because surface area and morphology impact how microparticles interact with the environment, controlling these properties is important. For example, specific shapes can improve cellular uptake, particle dissolution, or chemical catalysis.[5−7] Common methods for large-scale microparticle synthesis include solvent extraction or evaporation and dispersion polymerization.[8,9] These techniques are stochiometric in nature and thus provide limited control over particle size, shape, and chemistry and tend to make spherical particles.

Microfluidics provide excellent control over particle size and can fabricate particles with a broad range of shapes and chemical features, because they allow distinct reagents to be combined with precision timing and flow geometry.[10−12] Stop-flow lithography, for instance, can produce discs, triangles, and squares, labeled with distinctive chemical and optical features.[13,14] Alternatively, droplet-based templating uses microfluidics to form droplets of controlled size and structure that are transformed into solid particles through polymerization or gelation.[15,16] The simplest approach uses emulsion droplets dispersed in an immiscible carrier phase, such as water droplets in oil.[16] Alternatively, multiple emulsions and aqueous two-phase systems form droplets of nested semimiscible phases that yield a rich pastiche of particle shapes, sizes, and core−shell structures.[15,17−19] While it is thus possible to form particles with a variety of shapes using these techniques, all are essentially spherical, with the most extreme being bipolar ellipsoids.[15] A currently inaccessible but useful shape space would be particles with sharp edges and comprising surfaces with distinctive functionality, which would enable engineering of novel physical properties, like abrasiveness, angle of repose, and complex fluid flow.[20,21]

In this paper, we describe a droplet templating approach for making polyhedral particles with controlled size, concavity, and number of surfaces. We use microfluidics to form droplets of controlled size that are deformed into polyhedra of controlled concavity and then solidified. Deformation is achieved by compressing the emulsion via centrifugation during the gelling reaction, generating flat plateau borders between adjacent droplets that are locked-in via gelation. By controlling centrifugation speed, we control the degree of compression. By adding "indentation particles" comprising already solid particles, we create concave faces. By varying indentation particle size and number, we generate a variety of polyhedral particles with distinct shape and concavity. These particles should be useful for single cell encapsulation by particle-templated emulsification, DNA-encoded library screening, and soft materials rheology.

MATERIALS AND METHODS

Fabrication of polydimethylsiloxane (PDMS) drop generators is performed by mixing an 11:1 monomer to cross-linker ratio

Received: November 10, 2021
Accepted: March 31, 2022
Published: May 17, 2022

https://doi.org/10.1021/acs.analchem.1c04884
Anal. Chem. 2022, 94, 7475−7482

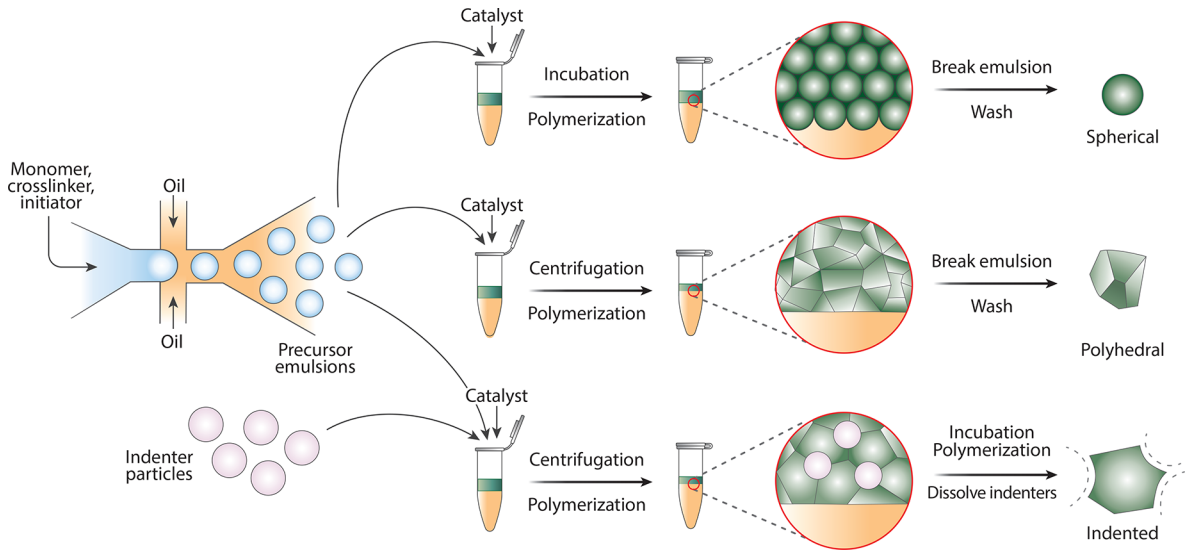

Figure 1. Indentation templating produces particles with controlled concavity. (Left) Microfluidics produces spherical droplets of controlled size containing gelling agents. (Top) Gelling the droplets yields common spherical particles. (Middle) By compressing the emulsion via centrifugation, the spherical droplets are deformed into polyhedra, yielding polyhedral particles upon gelation. (Bottom) To produce particles with concave interfaces, we add solid "indenter particles" and compress the emulsion during gelation.

and pouring over a silicon wafer presenting a photolithographically patterned layer of photoresist (SU-8 3025, MicroChem). Subsequent overnight curing at 80 °C, scalpel excision, inlet punching using a 0.75 mm biopsy punch (World Precision Instruments, #504529), oxygen plasma treatment, and bonding to a glass slide completes fabrication. An Aquapel (PPG Industries) treatment and incubation at 80 °C for 1 h ensures channel hydrophobicity.

The generation of all emulsions is performed using microfluidic drop generators and an oil phase consisting of 2% (w/w) perfluoropolyether−polyethelene glycol triblock copolymer (PFPE−PEG−PFPE) in Novec-7500 Engineering Fluid (3M). For small (35 μm) indenters, both the acrylamide solution and oil are run at 200 μL/h in an 18 μm channel. We prepare both precursor (45 μm) and large (85 μm) indenters using 500 or 1000 μL/h acrylamide solution flow rates, respectively, with 1000 μL/h oil flow rates in a 45 μm channel. Acrylamide solutions consist of two formulations to vary the elastic moduli. Both large and small indenters use 50 mM Tris-HCl pH 8.0 (Sigma-Aldrich), 1 mM EDTA (Sigma-Aldrich), 15 mM NaCl (Sigma-Aldrich), 32% (m/v) acrylamide (Sigma-Aldrich), 2.8% (m/v) N,N′-bis(acryloyl)cystamine (BAC; Sigma-Aldrich), and 0.3% (m/v) ammonium persulfate (Sigma-Aldrich). Precursor acrylamide solutions use 50 mM Tris-HCl pH 8.0, 1 mM EDTA, 15 mM NaCl, 6.2% acrylamide, 0.1% fluorescein *O*,*O*′-dimethacrylate (Sigma-Aldrich), *N*′,*N*′-methylenebis(acrylamide) (BIS; Sigma-Aldrich), and 0.3% ammonium persulfate. For indenter particles, the addition of 3% (v/v) TEMED (Invitrogen) to the oil initiates polymerization of the acrylamide solution with overnight mixing. For polyhedral particles, centrifugation at 2000 rcf for 1 h immediately follows the addition of 3% (v/v) TEMED with an additional incubation at 65 °C for 1 h following centrifugation. Following polymerization, the demulsification of all emulsions is achieved with the addition of perfluoro-1-octanol (Sigma-Aldrich) to a final concentration of 20% (v/v). Following demulsification, washing with 1% Span-80 in Hexane (Sigma-Aldrich) removes any remaining oil and surfactant from the particles. Three washes in a TBEST solution, consisting of 10 mM TrisHCl, 137 mM NaCl, 2.7 mM KCl (Sigma-Aldrich), 10 mM EDTA, and 0.1% Triton X100 (Sigma-Aldrich), and three washes in deionized water remove any unreacted acrylamide solution. The resulting particle geometry is identified using an EVOS FL Auto (ThermoFisher Scientific).

The encapsulation of fluorescently labeled beads (BD FACS Accudrop Beads, BD) using particle templated emulsification is evaluated using spherical, polyhedral, and indented particles. Briefly, the concentration of all particles is measured with a hemocytometer allowing for the preparation of aliquots consisting of 10k fluorescent beads, 0.5% (v/v) Triton X100, and 100k spherical particles in 1.5 mL tubes. Centrifugation of the aliquots at 6000 rcf for 1 min allows for the removal of the supernatant. Addition of 2% (w/w) PEG−PFPE amphiphilic block copolymer surfactant in Novec-7500 Engineering Fluid and vortexing results in emulsions with a diameter and geometry dependent on the spherical particle. For polyhedral particles, aliquots containing 10k fluorescent beads, 0.5% (v/v) Triton X100, 100k spherical particles, and 50% (v/v) glycerol (Sigma-Aldrich) allows for the generation of spherical emulsions using nonspherical polyhedral particles. With the addition of glycerol and removal of supernatant following centrifugation at 6000 rcf for 1 min, only moderate agitation by flicking was necessary to produce emulsions in the presence of 2% (w/w) PEG−PFPE amphiphilic block copolymer surfactant in Novec-7500 Engineering Fluid. In the case of indented particles, aliquots consist of only 10k fluorescent beads, 0.5% (v/v) Triton X100, and 100k spherical particles in 1.5 mL tubes. Following the centrifugation and removal of supernatant, the addition of 2% (w/w) PEG−PFPE amphiphilic block copolymer surfactant in Novec-7500 Engineering Fluid and gentle inversion is sufficient to generate emulsions. The distribution of particles, size, and number of encapsulated beads is evaluated using an EVOS FL Auto.

Droplet digital PCR was performed using *S. cerevisiae* genomic DNA (Millipore). A total of 48 μL of selected particles were hardpacked by centrifugation then suspended in 1× Platinum Hot Start Master Mix (Invitrogen), 0.9 μM

https://doi.org/10.1021/acs.analchem.1c04884
Anal. Chem. 2022, 94, 7475−7482

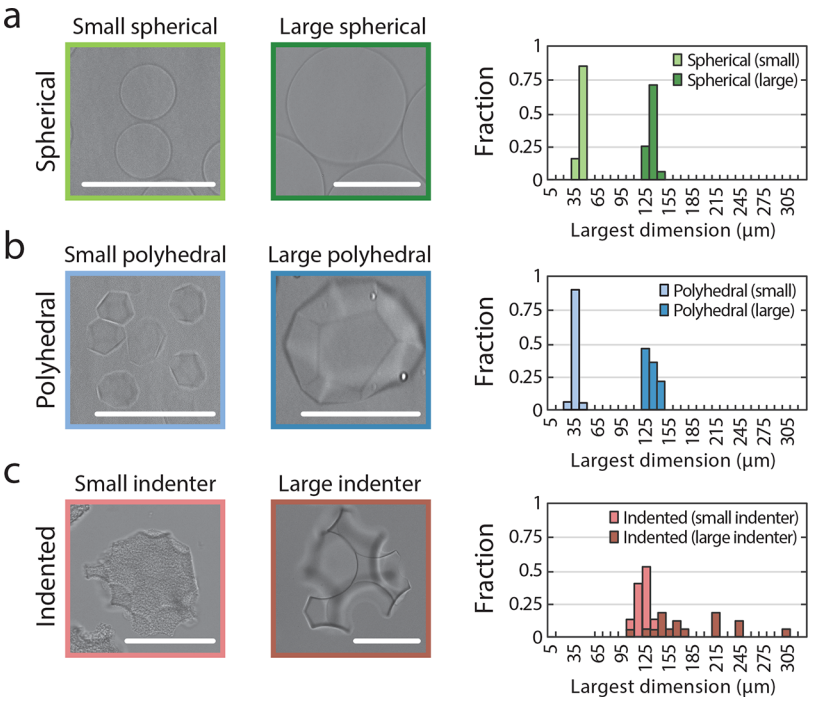

Figure 2. Indentation templating generates particles with controlled size and surface curvature. (a) Small (45 μm) and large (135 μm) spherical particles produced by gelling an uncompressed emulsion. (b) Polyhedral particles produced by compressing and gelling an emulsion. (c) Particles with concave faces produced by adding indenter particles to the emulsion prior to compression and gelation. The plots on the right are the particle size distributions, as measured for the particle longest axis. Even though the particles have low volume dispersity (<5%), the longest axes vary due to differences in particle shape. Scale bar: 100 μm.

forward primer (5′-GCAGACCAGACCAGAACAAA-3′, IDT), 0.9 μM reverse primer (5′-ACACGTATGTATCTAG-CCGAATAAC-3′, IDT), and 0.9 μM TaqMan probe (5′-/56-FAM/ATATGTTGT/ZEN/TCACTCGCGCCTGGG/3IABkFQ/-3′, IDT), and 1% (v/v) Triton X100. We mixed via vortexing and incubated at room temperature for 5 min under gentle agitation to promote diffusion. The selected particles were then centrifuged at 6000 rcf for 2 min to pellet, and the supernatant was removed. To each sample, 2 μL of diluted *S. cerevisiae* DNA was added and mixed via briefly vortexing and flicking the tubes. A total of 100 μL of 2% (w/w) PEG−PFPE amphiphilic block copolymer surfactant in Novec-7500 Engineering Fluid was added, and the samples were agitated according to their geometry. Spherical and polyhedral samples were vortexed, while indented particles were simply inverted. The resulting emulsions were thermocycled at 95 °C for 2 min, then 34 cycles of 95 °C for 30 s, 50 °C for 30 s, and 72 °C for 60 s, then a final extension at 72 °C for 2 min before a 4 °C hold. The droplets were imaged using an EVOS FL Auto. Positive and negative droplets were then counted with the number of targets calculated according to[22]

$$C = D\left(\frac{1}{TV}\right)\frac{\left(\log\left(1-\frac{P}{T}\right)\right)}{\left(\log\left(1-\frac{1}{T}\right)\right)} \quad (1)$$

where C is the concentration of targets, sample dilution is D, droplet volume is V, the total number of droplets is T, and the number of positive droplets is P.

RESULTS AND DISCUSSION

Droplet templating uses microfluidics to form droplets of controlled size and shape (Figure 1, left) that are transformed into particles by solidification. Solidification is often achieved by polymerization or cross-linking.[16,23] To generate polyacrylamide hydrogel particles, we include an acrylamide monomer, a bis-acrylamide cross-linker, and an ammonium per sulfate initiator in the droplet phase. The droplets remain liquid until the catalyst, tetramethylethylenediamine (TEMED), is introduced via the fluorinated carrier phase, in which it is partially soluble. To generate polyhedral particles, the emulsion must be compressed before the catalyst is introduced, which we do by centrifugation.

Under normal gravity, droplets in our emulsions are minimally compressed because the gravitational pressure due to buoyancy $G = \Delta\rho ah$, with $\Delta\rho$ being the difference in oil and droplet densities, a is the acceleration due to acceleration, and h is the height of the droplet layer, is small compared to the droplet Laplace Pressure $\Delta P = \frac{2\sigma}{r}$, with σ being the droplet interfacial tension and r being the droplet radius. Under these conditions, we thus generate spherical particles (Figure 1, top). Here, the dimensionless ratio of Laplace pressure (1.1 kPa) to gravitational pressure (6 Pa) is greater than one (183, dimensionless ratio), indicating minimal compression. When we centrifuge the emulsion, we increase gravitational relative to Laplace pressure such that the ratio is less than one; this expels oil between the droplets and causes deformation.[24] Neighboring droplets possessing similar Laplace Pressure push against each other resulting in a flat plateau border and "foamlike" emulsion. If the catalyst is added just before compression is applied, polymerization locks this geometry in place, yielding polyhedral particles with flat surfaces corresponding to interfaces with nearest neighbors. The number of faces indented on a particle thus equals the number of nearest neighbors, which depends on the relative sizes of the droplets

https://doi.org/10.1021/acs.analchem.1c04884
Anal. Chem. 2022, 94, 7475−7482

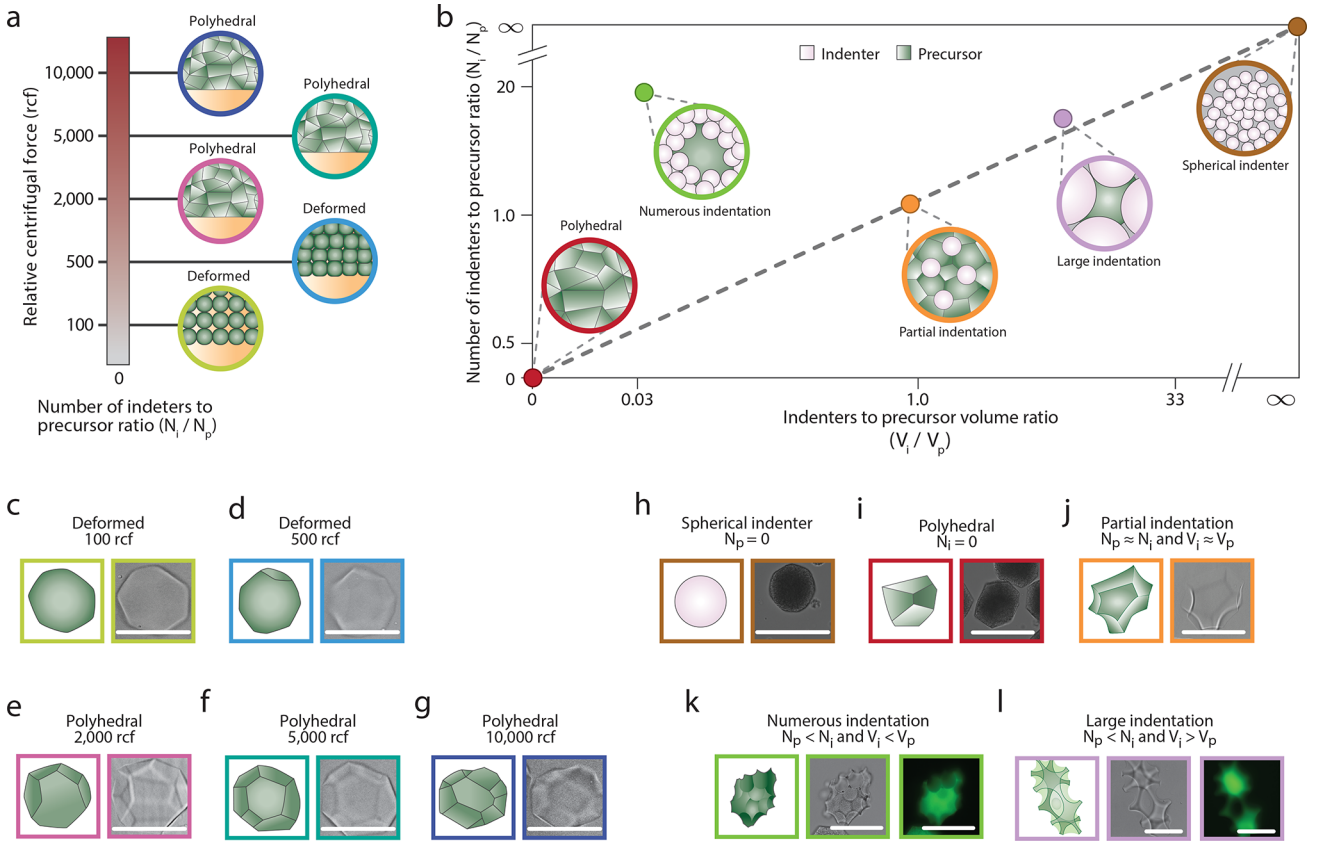

Figure 3. Indentation templating generates particles with controlled surface shape. (a) Effect of centrifugal force on droplet geometry. (b) Map depicting particles generated by varying the ratio of droplets and indenter particles in the solidified emulsion. (c) Minimal deformation observed under 100 rcf for polyhedral particles (N_i/N_p = 0). (d) Similarly minimal deformation observed under 500 rcf for polyhedral particles. (e) Deformation observed at 2000 rcf for polyhedral particles. (f) Polyhedral particle deformation at 5000 rcf. (g) Deformation at 10000 rcf, notably similar to both 5000 and 2000 rcf. (h) Spherical particles (N_p = 0), (i) polyhedral particles (N_i = 0), (j) partial particles ($V_i = V_p$ and $N_i = N_p$), (k) small indented particles ($V_i < V_p$ and $N_i > N_p$), and (l) large, indented particles ($V_i > V_p$ and $N_i > N_p$. Scale bar: 100 μm

(Figure 1, middle). We expect this to follow closed packing with an average of 12 nearest neighbors with minor variation in the number of neighbors due to the nature of packing and centrifugation. For mixtures of two or more differently sized droplets, we expect this variation to be larger.

For droplets of identical composition and size, the interfaces are flat, because the Laplace pressures of adjacent droplets are equal. To generate a concave interface requires indentation by an object with a modulus larger than the droplet's Laplace pressure. This can be achieved by adding already-solid particles to the emulsion prior to compression. These "indenter particles" have elastic moduli exceeding 1 MPa, which is larger than the Laplace pressure of the droplets. During compression, the particles indent the droplets, generating concave faces (Figure 1, bottom). With this approach, the curvature of the resulting face depends on the indenter size and modulus and degree of compression. The indenter particles are cross-linked via *N*,*N*′-bis(acryloyl)cystamine, which can be reversed via addition of a reducing agent such as dithiothreitol; postpolymerization, this allows the dissolution of indenters, leaving behind just the polyhedral particles.

To characterize the control afforded by indentation templating, we image particles generated under different conditions and measure the resultant size distributions. For each condition, we generate small and large particles. Without compression, we obtain monodispersed spherical particles with average diameters 41 ± 1 μm (small) or 133 ± 6 μm (large; Figure 2a). When we apply compression, we obtain uniform polyhedra with flat surfaces; we characterize these particles by their longest dimension, obtaining average sizes of 41 ± 3 (small) and 122 ± 7 μm (large; Figure 2b, right). We measure an average of 11.5 ± 1.1 flat surfaces for small particles and 11.6 ± 1.4 flat surfaces for large particles. This confirms low variability in the number of flat surfaces per particle and that the number of nearest neighbors is independent of size. The narrow size distribution suggests minimal coalescence during centrifugation, since coalescence is favored during separation rather than compression of droplets.[25,26] When we include indenters we obtain particles with curved surfaces in which concavity depends on indenter size. For indenters of 34 ± 3 μm applied to droplets of 81 ± 1 μm, we obtain particles of 120 ± 7 μm with multiple concavities of the inverse curvature of the indenters and a narrow size distribution (light orange, Figure 2c). For indenters of 121 ± 7 μm applied to droplets of 81 ± 1 μm, we obtain high surface area particles of 182 ± 54 μm with numerous large indentations (dark orange, Figure 2c). These particles form in the spaces between packed indenters and thus have a high surface area and shape that depends on the local packing structure.

Indentation templating can thus generate particles with a variety of sizes, shapes, and concavity curvatures. Centrifugation is an important parameter in indentation templating (Figure 3a). Centrifugation insufficient to overcome the Laplace pressure of the droplets results in minimal deformation

https://doi.org/10.1021/acs.analchem.1c04884
Anal. Chem. 2022, 94, 7475−7482

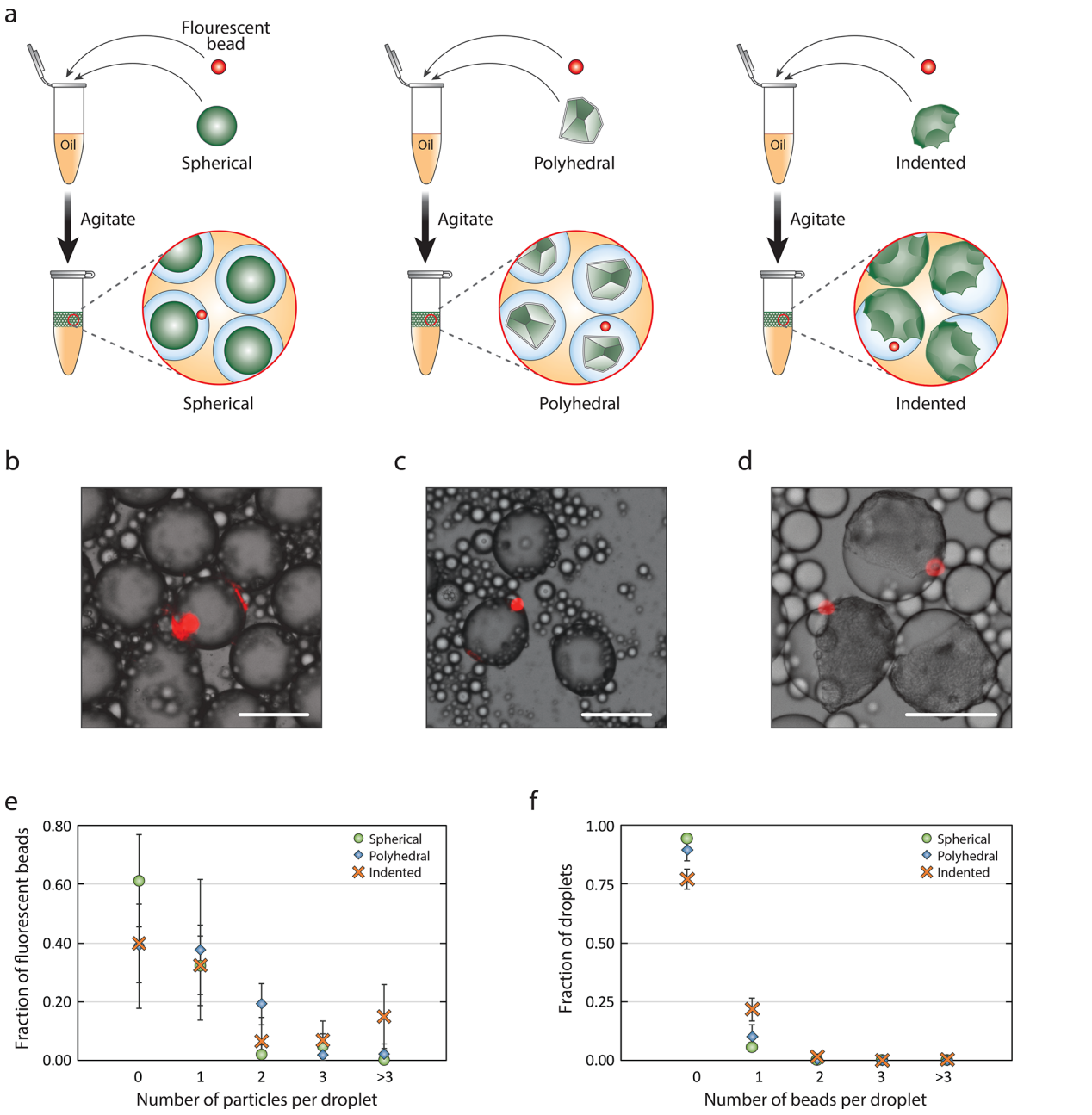

Figure 4. Templating particle shape affects emulsification. (a) Example templating particle shapes and (b–d) images of resultant emulsions. (e) Fraction of fluorescent beads encapsulated in droplets versus number of templating particles per droplet. (f) Fraction of droplets that contain fluorescent beads vs number of templating particles per droplet. Scale bar: 100 μm

(Figure 3a,c,d). Likewise, centrifugation beyond the Laplace pressure has minimal impact due to volumetric confinement and the incompressibility of the precursor liquid (Figure 3a,e–g). The primary parameters that control particle properties are the indenter to droplet number ratio $\frac{N_i}{N_p}$ and volume ratio $\frac{V_i}{V_p}$ (Figure 3b). Without droplets, there are only indenter particles (Figure 3h), while without indenters we observe only polyhedra with flat faces ($N_i = 0$ or $V_i = 0$, Figure 3i). For equally sized indenters and precursors ($V_i = V_p$) at an equal ratio ($N_i = N_p$), we observe flat and concave curvatures corresponding to contact with droplets or indenters, respectively (Figure 3j). When indenters outnumber droplets ($N_i > N_p$), we obtain high surface area particles with a few large indentations ($V_i > V_p$, Figure 3l) or many small ones ($V_i < V_p$, Figure 3k). The surface curvature can be controlled by the size ratio of indenters to precursors. These results demonstrate the ability to generate polyhedral particles with a range of shape and concavity properties using indentation templating.

Particle-templated emulsification (PTE) allows analysis of molecules and cells in droplet reactions without the need for microfluidics; this increases the accessibility of these powerful assays for laboratories lacking microfluidic expertise.[27] In the approach, particles are mixed with the sample, oil is added, and the mixture agitated to generate an emulsion. Normally, this would yield a polydispersed monomodal emulsion, but the presence of the particles results in a bimodal distribution comprising small polydispersed droplets mixed with large uniform ones containing the particles. Under ideal conditions, the particle-containing droplets encapsulate most of the

https://doi.org/10.1021/acs.analchem.1c04884
Anal. Chem. 2022, 94, 7475–7482

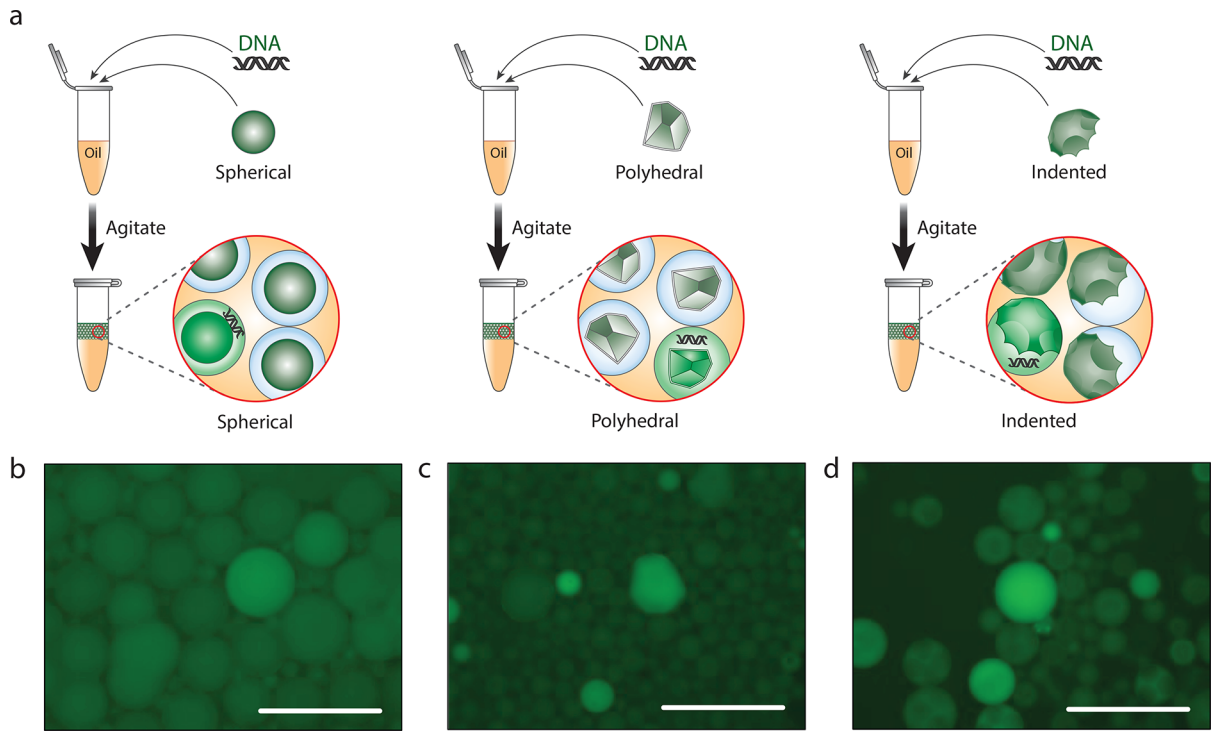

Figure 5. Droplet digital PCR using polyhedral and indented particles. (a) We encapsulate both yeast genomic DNA and ddPCR reagents in droplets using PTE. Observation of positive ddPCR droplets associated with (b) spherical, (c) polyhedral, and (d) indented particles allows for calculation of the targets within samples. Scale bar: 200 μm.

sample, thereby maximizing the amount partitioned with a particle and thus yielding a fruitful assay. Sample encapsulation efficiency is thus a key parameter in PTE.

To date, PTE has been performed exclusively with spherical particles, even though shape likely impacts encapsulation efficiency, and spheres may not be optimal. Our indented particles thus provide an opportunity to investigate how shape effects this process and may enable increased encapsulation efficiency. To investigate this, we encapsulate samples via PTE using particles of different shape formed by indentation templating. To assess sample encapsulation efficiency, we include fluorescent beads clearly visible in the droplets postencapsulation (Figure 4a). For spherical hydrogels (Figure 4b), 39 ± 16% of fluorescent beads are encapsulated (Figure 4e), and the droplets have an aqueous volume fraction of 0.1 (supplemental). For polyhedral particles (Figure 4a, middle), we obtain a similar emulsion (Figure 4c) with 61 ± 21% of beads encapsulated (Figure 4e) and an aqueous volume fraction of 0.07. In contrast to both spheres and polyhedra, particles indented with numerous small concavities (Figure 4a, right) require no agitation to generate the emulsion beyond addition of oil by pipet. The result is an aqueous volume fraction of 0.48 with 60 ± 16% of fluorescent beads encapsulated (Figure 4e). This suggests that the increase in droplet size and the reduction in agitation for emulsification is of direct benefit to PTE. Interestingly, these particles appear to adhere to the droplet interface, which implies affinity for the oil that may result from surfactant entrapment at the particle interface during polymerization.[28] While this entrapment likely occurs for all shapes, we only observe it for particles with concavities. This implies that oil affinity and, thus, degree of chemical functionalization depend on interface curvature.

Particle shape influences the properties of emulsions generated by PTE and, thus, may impact the efficiency with which sample is encapsulated. To investigate this, we compare the fraction of beads encapsulated in droplets containing hydrogel particles of different shape. For spheres, we find that 9 ± 3% of beads end up in hydrogel droplets. For polyhedra, this increases to 16 ± 16% and for highly indented particles 23 ± 5% illustrating that, indeed, sample encapsulation efficiency increases with volume fraction and, thus, is impacted by particle shape (Figure 4f). These numbers depend on the specific conditions under which PTE is applied and, thus, the droplet contents, fluid properties like viscosity and interfacial tension, and mechanism of agitation. However, intuitively, and for the conditions tested, nonspherical particles with concavities have higher encapsulation efficiency than other shapes.

Droplet digital PCR (ddPCR) uses microfluidics to encapsulate single molecules of DNA for amplification. ddPCR offers direct quantification, increased sensitivity, and improved detection.[29,30] Particle-templated emulsification allows for a microfluidic-free method of encapsulation for ddPCR.[31] Here we investigate the effects of different particle geometries on the detection and quantification of yeast genomic DNA using ddPCR. We observe that all particle geometries are compatible with ddPCR (Figure 5b–d). Based on these ddPCR results, we calculate a target concentration of three targets per pL for spherical particles, six targets per pL for polyhedral, and two targets per pL for indented particles for a sample estimated at two targets per pL. Additionally, we observe a brighter signal using nonspherical particles. This suggests an improved efficiency of the PCR reaction with these particles when compared to standard spherical particles.

https://doi.org/10.1021/acs.analchem.1c04884
Anal. Chem. 2022, 94, 7475−7482

CONCLUSIONS

Indentation templating affords a controlled and flexible means by which to engineer the shape of microparticles. As we have shown, a broad array of shapes can be generated by varying relative sizes and numbers of the precursor droplets and indentation particles. It uses high throughput microfluidics to form the indenter and precursor droplets that can be scaled up via bubble-triggered droplet generation and parallelization.[32] Particle shaping is accomplished with bulk centrifugation and is even more scalable. Thus, the approach is as scalable as processes for forming particles that can generate liters per day.[32]

While we have focused on the fabrication of compliant hydrogels, the concept should apply to chemistries yielding hard particles,[33,34] provided they are compatible with emulsification, chemical solidification, and emulsion stability under compression. Moreover, because solidification occurs while droplets and indenters are in contact, it should be possible to functionalize different faces by including mixtures of indenter and droplet chemistries in the emulsion during the solidification reaction,[35,36] with these functionalities matched to the curvatures of their complementary faces. Looking forward, we envision that particles with a more extreme geometry and spatially varied chemical functionalization will be possible using indentation templating. For example, pushing size and number ratios to the extreme should generate high aspect ratio particles and sheets with a reticulated foamlike structure.[37]

A current limitation of our approach is that while size and average structure are well controlled, the particles are not identical. This is due to particles forming in a randomly packed emulsion. To increase uniformity, methods for ordering the pack into crystalline arrays can be employed, resulting in a global structure that will yield identical particles. For example, seeding templates can arrange colloids into ordered arrays over sizable length scales,[38] yielding particles with uniform, intricately controlled shape. Moreover, these approaches can generate crystals with different lattices,[39] yielding particles of lattice-complementary shape.

Indentation templating thus provides a rich palette for engineering particle shape and chemistry to optimize for novel applications. For example, in the field of droplet assays, polyhedra with controlled concavity should be useful for increasing the efficiency of molecule and cell encapsulation.[40,41] When used as substrates for chemical catalysis, particles with curved, functional interfaces may afford control over chemical transformation rates, with different faces functionalized with moieties, dyes, and catalysts that yield multifunctional particles.[42,43] In addition, sharp edges and tunable sphericity should impart unique rheological and flow properties, while particle mixtures can be included in matrices to generate novel soft materials.[44]

AUTHOR INFORMATION

Corresponding Author

Adam R. Abate − *Department of Bioengineering and Therapeutic Sciences, University of California, San Francisco, San Francisco, California 94158, United States; Chan Zuckerberg Biohub, San Francisco, California 94158, United States;* orcid.org/0000-0001-9614-4831; Email: adam@abatelab.org

Authors

Daniel W. Weisgerber − *Department of Bioengineering and Therapeutic Sciences, University of California, San Francisco, San Francisco, California 94158, United States;* orcid.org/0000-0003-3187-634X

Makiko Hatori − *Department of Bioengineering and Therapeutic Sciences, University of California, San Francisco, San Francisco, California 94158, United States*

Xiangpeng Li − *Department of Bioengineering and Therapeutic Sciences, University of California, San Francisco, San Francisco, California 94158, United States*

Complete contact information is available at: https://pubs.acs.org/10.1021/acs.analchem.1c04884

Notes

The authors declare no competing financial interest.

ACKNOWLEDGMENTS

This work developing this protocol was supported by the National Institutes of Health (R01-EB019453-02 and U01-AI129206-01), the Office of the Director of National Intelligence, Intelligence Advanced Research Projects Activity (IARPA) under Contract No. N66001-18-C-4507, the Chan-Zuckerberg Biohub Investigator Program, Defense Advanced Research Projects Agency (DARPA) under Contract No. W911NF1920013, and Virology Surveillance and Diagnosis Branch, Influenza Division, Centers for Disease Control and Prevention, under BAA 75D301-19-R-67835 (Topic #6). The content of the information does not necessarily reflect the position or the policy of the Government, and no official endorsement should be inferred.

REFERENCES

(1) Vilos, C.; Velasquez, L. A. *J. Biomed. Biotechnol.* **2012**, *2012*, 1.
(2) Kozlowska, J.; Prus, W.; Stachowiak, N. *Int. J. Biol. Macromol.* **2019**, *129*, 952.
(3) Ye, C.; Chen, A.; Colombo, P.; Martinez, C. *J. R. Soc. Interface* **2010**, *7*, 7.
(4) Javadi, A.; Zhao, J.; Cao, C.; Pozuelo, M.; Yang, Y.; Hwang, I.; Lin, T. C.; Li, X. *Sci. Rep.* **2017**, *7*, 7.
(5) He, Y.; Park, K. *Mol. Pharmaceutics* **2016**, *13*, 2164.
(6) Cao, S.; Tao, F.; Tang, Y.; Li, Y.; Yu, J. *Chem. Soc. Rev.* **2016**, *45*, 4747.
(7) Graf, C.; Nordmeyer, D.; Sengstock, C.; Ahlberg, S.; Diendorf, J.; Raabe, J.; Epple, M.; Köller, M.; Lademann, J.; Vogt, A.; Rancan, F.; Rühl, E. *Langmuir* **2018**, *34*, 1506.
(8) Pu, M.; Liu, K.; Zhang, M.; Yuan, P.; Cai, J. *Ind. Eng. Chem. Res.* **2020**, *59*, 2892.
(9) Wang, W.; Griffiths, R. M. T.; Naylor, A.; Giles, M. R.; Irvine, D. J.; Howdle, S. M. *Polymer* **2002**, *43*, 6653.
(10) Qiu, Y.; Wang, F.; Liu, Y.-M.; Wang, W.; Chu, L.-Y.; Wang, H.-L. *Sci. Rep.* **2015**, *5*, 5.
(11) Kim, D.-Y.; Jin, S. H.; Jeong, S.-G.; Lee, B.; Kang, K.-K.; Lee, C.-S. *Sci. Rep.* **2018**, *8*, 8.
(12) Del Giudice, F.; D'Avino, G.; Maffettone, P. L. *Lab Chip* **2021**, *21*, 2069−2094.
(13) Dendukuri, D.; Gu, S. S.; Pregibon, D. C.; Hatton, T. A.; Doyle, P. S. *Lab Chip* **2007**, *7*, 818.
(14) Nam, S. M.; Kim, K.; Kang, I.-S.; Park, W.; Lee, W. *Bio Chip J.* **2019**, *13*, 226.
(15) Wang, J.; Li, Y.; Wang, X.; Wang, J.; Tian, H.; Zhao, P.; Tian, Y.; Gu, Y.; Wang, L.; Wang, C. *Micromachines* **2017**, *8*, 22.
(16) Li, W.; Zhang, L.; Ge, X.; Xu, B.; Zhang, W.; Qu, L.; Choi, C.-H.; Xu, J.; Zhang, A.; Lee, H.; Weitz, D. A. *Chem. Soc. Rev.* **2018**, *47*, 5646.

(17) Yu, L.; Sun, Q.; Hui, Y.; Seth, A.; Petrovsky, N.; Zhao, C.-X. *J. Colloid Interface Sci.* **2019**, *539*, 497.
(18) Xu, S.; Nie, Z.; Seo, M.; Lewis, P.; Kumacheva, E.; Stone, H. A.; Garstecki, P.; Weibel, D. B.; Gitlin, I.; Whitesides, G. M. *Angew. Chem., Int. Ed.* **2005**, *44*, 724.
(19) Shepherd, R. F.; Conrad, J. C.; Rhodes, S. K.; Link, D. R.; Marquez, M.; Weitz, D. A.; Lewis, J. A. *Langmuir* **2006**, *22*, 8618.
(20) Hayakawa, M.; Onoe, H.; Nagai, K. H.; Takinoue, M. *Sci. Rep.* **2016**, *6*, 6.
(21) Gao, Y.; van Reenen, A.; Hulsen, M. A.; de Jong, A. M.; Prins, M. W. J.; den Toonder, J. M. J. *Microfluid Nanofluid* **2014**, *16*, 265.
(22) Corbisier, P.; Pinheiro, L.; Mazoua, S.; Kortekaas, A.-M.; Chung, P. Y. J.; Gerganova, T.; Roebben, G.; Emons, H.; Emslie, K. *Anal. Bioanal. Chem.* **2015**, *407*, 1831−1840.
(23) Yu, L.; Sun, Q.; Hui, Y.; Seth, A.; Petrovsky, N.; Zhao, C.-X. *J. Colloid Interface Sci.* **2019**, *539*, 497.
(24) Ershov, D.; Sprakel, J.; Appel, J.; Cohen Stuart, M. A.; van der Gucht, J. *Proc. Natl. Acad. Sci. U.S.A.* **2013**, *110*, 9220.
(25) Bremond, N.; Thiam, A. R.; Bibette, J. *Phys. Rev. Lett.* **2008**, *100*, 024501.
(26) Manica, R.; Connor, J. N.; Dagastine, R. R.; Carnie, S. L.; Horn, R. G.; Chan, D. Y. C. *Phys. Fluids.* **2008**, *20*, 032101.
(27) Hatori, M. N.; Kim, S. C.; Abate, A. R. *Anal. Chem.* **2018**, *90*, 9813.
(28) Liu, L.; Li, P.; Asher, S. A. *Nature* **1999**, *397*, 141.
(29) Olmedillas-López, S.; García-Arranz, M.; García-Olmo, D. *Mol. Diagn. Ther* **2017**, *21*, 493−510.
(30) Mashaghi, S.; Abbaspourrad, A.; Weitz, D. A.; van Oijen, A. M. *Trends Analyt. Chem.* **2016**, *82*, 118−125.
(31) Yan, Z.; Clark, I. C.; Abate, A. R. *Macromol. Chem. Phys.* **2017**, *218*, 1600297.
(32) Yadavali, S.; Jeong, H.-H.; Lee, D.; Issadore, D. *Nat. Commun.* **2018**, *9*, 9.
(33) Zhang, M.; Wang, W.; Xie, R.; Ju, X.; Liu, Z.; Jiang, L.; Chen, Q.; Chu, L. *Particuology* **2016**, *24*, 18.
(34) Ye, C.; Chen, A.; Colombo, P.; Martinez, C. *J. R. Soc. Interface* **2010**, *7*, 7.
(35) Ren, W.; Wen, S.; Tawfik, S. A.; Su, Q. P.; Lin, G.; Ju, L. A.; Ford, M. J.; Ghodke, H.; van Oijen, A. M.; Jin, D. *Chem. Sci.* **2018**, *9*, 4352.
(36) Gruner, P.; Riechers, B.; Semin, B.; Lim, J.; Johnston, A.; Short, K.; Baret, J.-C. *Nat. Commun.* **2016**, *7*, 7.
(37) Kersey, F. R.; Merkel, T. J.; Perry, J. L.; Napier, M. E.; DeSimone, J. M. *Langmuir* **2012**, *28*, 8773.
(38) Yin, Y.; Lu, Y.; Gates, B.; Xia, Y. *J. Am. Chem. Soc.* **2001**, *123*, 8718.
(39) Mazid, R. R.; Si, K. J.; Cheng, W. *Methods* **2014**, *67*, 215.
(40) Barua, S.; Yoo, J.-W.; Kolhar, P.; Wakankar, A.; Gokarn, Y. R.; Mitragotri, S. *Proc. Natl. Acad. Sci. U.S.A.* **2013**, *110*, 3270.
(41) Arno, M. C.; Inam, M.; Weems, A. C.; Li, Z.; Binch, A. L. A.; Platt, C. I.; Richardson, S. M.; Hoyland, J. A.; Dove, A. P.; O'Reilly, R. K. *Nat. Commun.* **2020**, *11*, 11.
(42) Walther, A.; Müller, A. H. E. *Chem. Rev.* **2013**, *113*, 5194.
(43) Hu, J.; Zhou, S.; Sun, Y.; Fang, X.; Wu, L. *Chem. Soc. Rev.* **2012**, *41*, 4356.
(44) Daly, A. C.; Riley, L.; Segura, T.; Burdick, J. A. *Nat. Rev. Mater.* **2020**, *5*, 20.

https://doi.org/10.1021/acs.analchem.1c04884
Anal. Chem. 2022, 94, 7475−7482